Supplementary Material for

Extent of impact of deep-sea nodule mining midwater plumes is influenced by sediment loading, turbulence and thresholds

Carlos Munoz-Royo[1*], Thomas Peacock[1*], Matthew H. Alford[2], Jerome A. Smith[2], Arnaud Le Boyer[2], Chinmay S. Kulkarni[1], Pierre F.J. Lermusiaux[1], Patrick J. Haley Jr.[1], C. Mirabito[1], Dayang Wang[1], E. Eric Adams[1], Raphael Ouillon[1],Alexander Breugem[3], Boudewijn Decrop[3], Thijs Lanckriet[4], Rohit B. Supekar[1], Andrew J. Rzeznik[1], Amy Gartman[5], and Se-Jong Ju[6].

[1] *Massachusetts Institute of Technology, Cambridge, Massachusetts, USA.*

[2] *Scripps Institution of Oceanography, University of California, La Jolla, California, USA.*

[3] *International Marine and Dredging Consultants, Antwerp, Belgium.*

[4] *Fluves, Ghent, Belgium.*

[5] *U.S. Geological Survey, PCMSC, Santa Cruz, California, USA.*

[6] *Korea Institute of Ocean Science and Technology, Busan, Republic of Korea.*

** Corresponding authors: carlosmr@mit.edu, tomp@mit.edu*

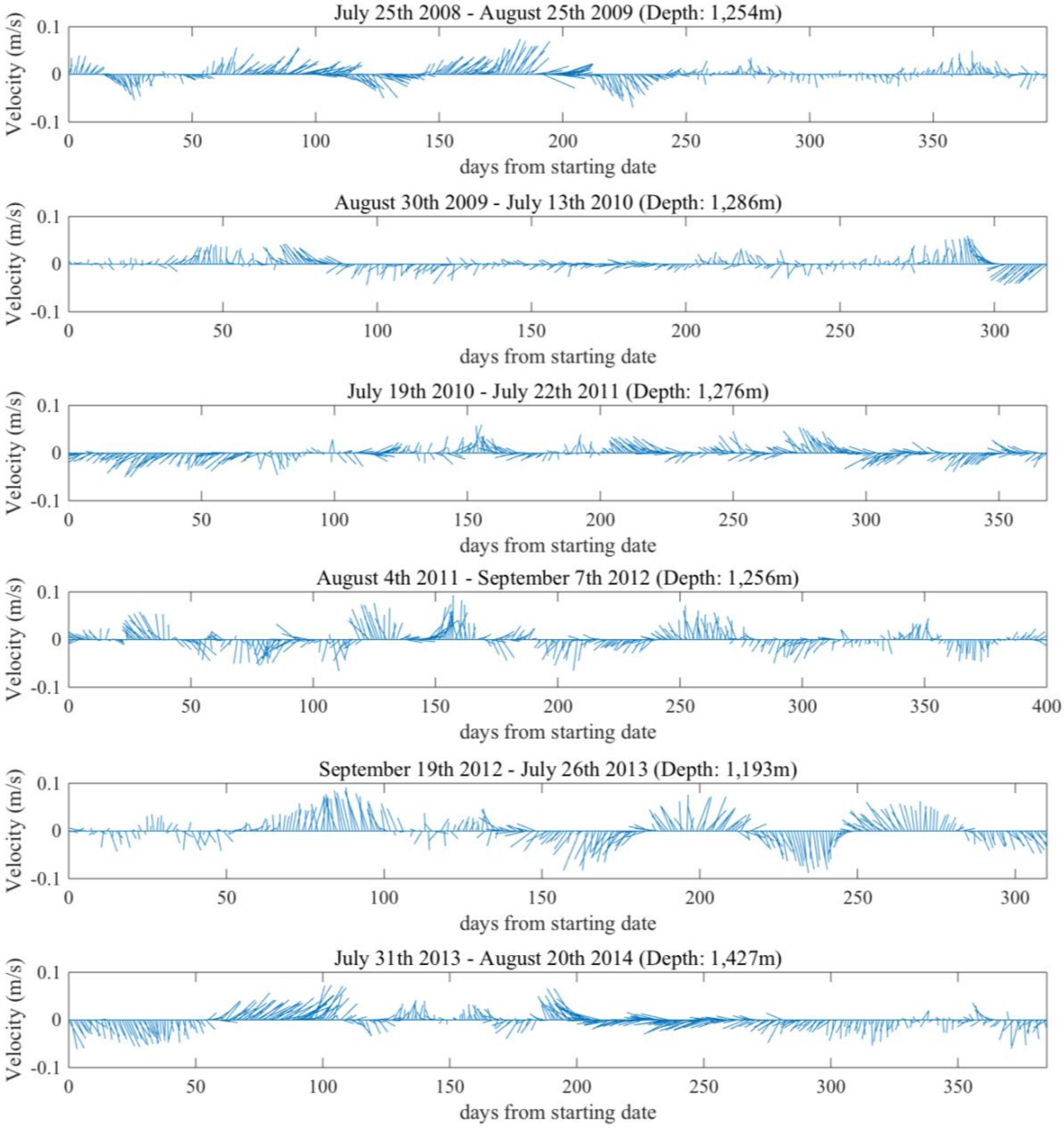

Supplementary Figure 1. *6-year time series of daily average current velocity and heading measured at depths between 1193 m and 1427 m in the Korean exploration licensed area in the CCFZ (10º 30'N 131º 20'W). The maximum observed daily average velocity was 0.11m* s^{-1}*, and the mean was 0.04m* s^{-1} *over the 6-year period. The current velocity and heading were measured using a single point current meter SeaGuard RCM DW (Aanderaa).*

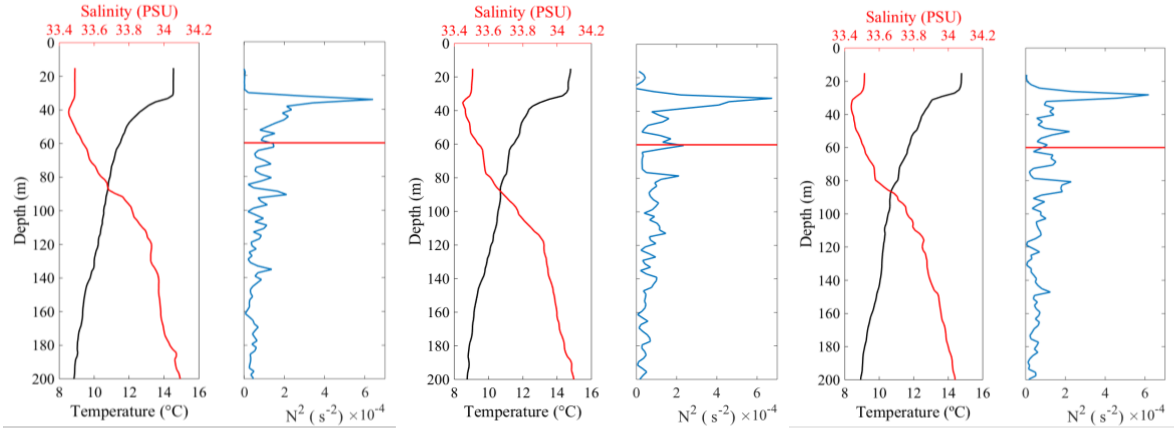

Supplementary Figure 2. *Sample salinity, temperature and buoyancy frequency (N^2) profiles measured before the release of Saltwater plume 1, CCFZ sediment plume and Saltwater plume 2, respectively from left to right. The horizontal red line in the buoyancy frequency plots indicates the plume discharge depth, which was well below the mixed layer. The conductivity, temperature and depth were measured by an SBE911plus CTD sensor.*

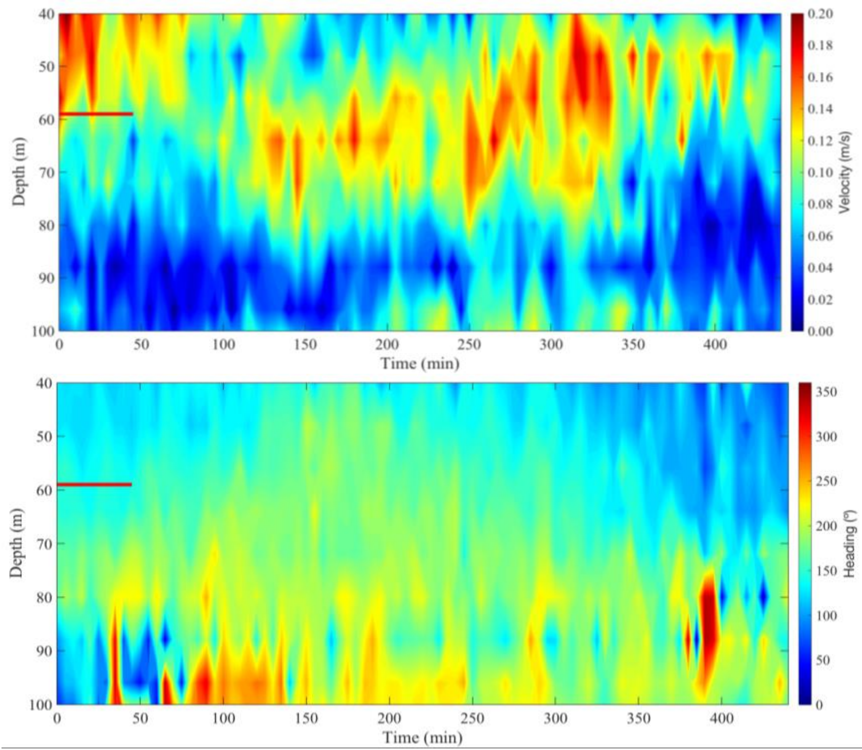

Supplementary Figure 3. *Current velocity (top) and heading (bottom) during the release (first 45 minutes) and tracking (from minute 45 to 440) of the CCFZ sediment plume. The horizontal red line indicates the plume discharge depth (59m) and time (45 minutes). During the discharge, the current affecting the dynamic plume descending from 60m to ~72m of depth was below 0.12m s^{-1} and with a constant heading.*

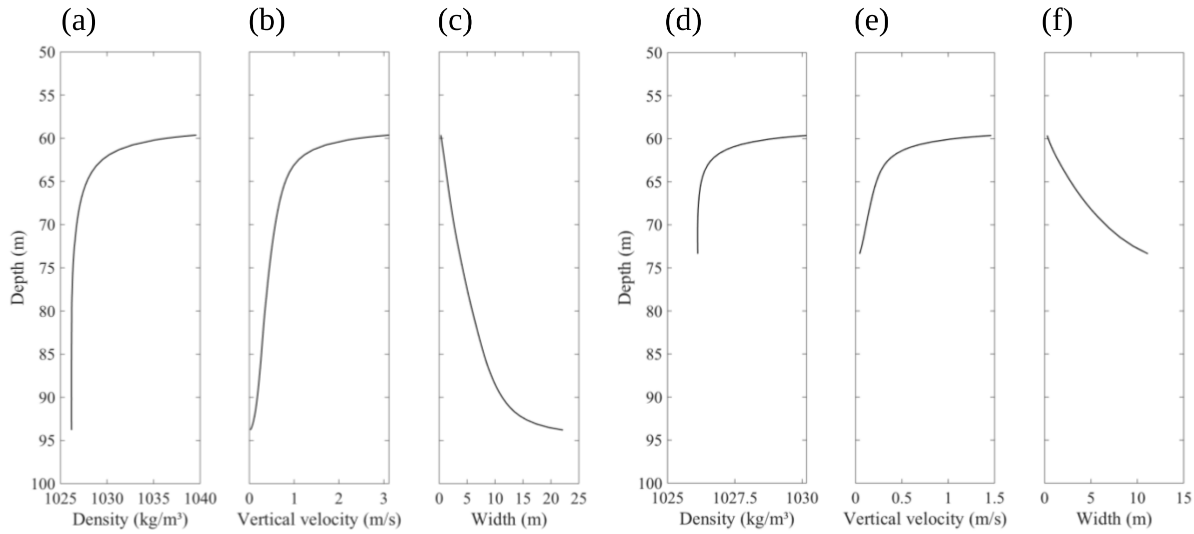

Supplementary Figure 4. *Saltwater plume 1 (a) density, (b) vertical velocity and (c) width profiles obtained using DP1 model. CCFZ sediment and saltwater 2 plume (d) density, (e) vertical velocity and (f) width profiles obtained using DP1 model.*

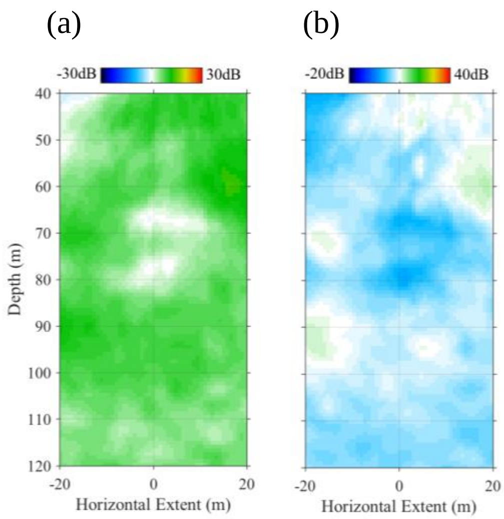

Supplementary Figure 5. *Ocean background acoustic backscatter measured by the PADS using two different color scales (a-b). To minimize the ocean background signal and present a clearer imaging of the plume, the color scale of (b) is the one used in Figure 2.*

Supplementary Notes 1.

Epsilometer vertical profile

The plume core as detected by the epsilometer was centered around 73-74 m (Figure 3 and Supplementary Figure 6), which is slightly deeper than the initial 68 m depth detection during the tow-yo (Figure 5). This is because the epsilometer measurements were very close (~30 m) to the release and, therefore, still during the rebound of the dynamic plume from its maximum depth. It is also the case that there is about 1 hour time difference between the epsilometer profiles and the initial tow-yo data (Figure 5), on which time the background heaving of isopycnals could account for a +/-5 m displacement, as observed in Figure 5.

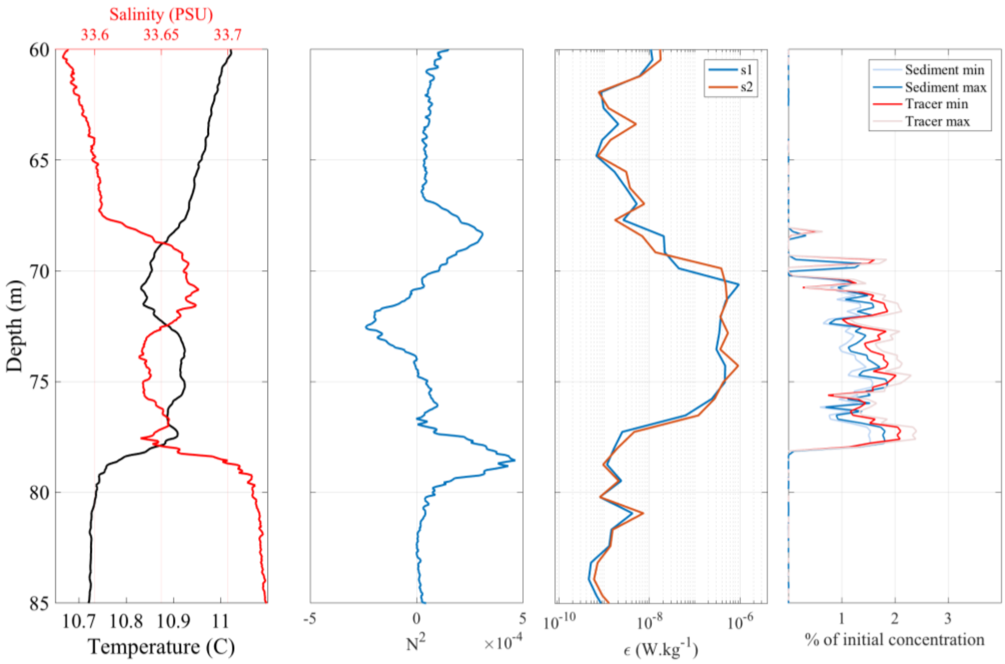

Supplementary Figure 6*. A second example of a vertical profile measured with the epsilometer during the discharge of the CCFZ sediment plume. In the results section of the article, the data from another epsilometer downcast during the CCFZ sediment plume discharge is presented (Figure 3).*

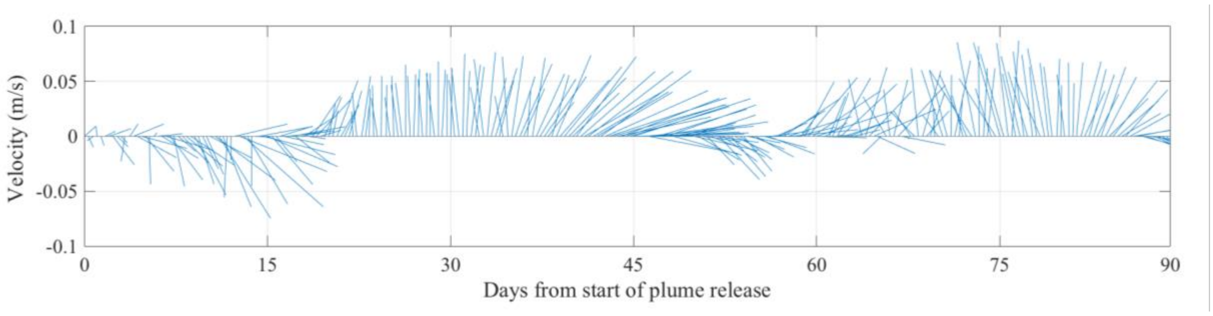

Supplementary Figure 7. *TELEMAC model current velocity and direction at the location and depth (1000 m) of the plume source.*

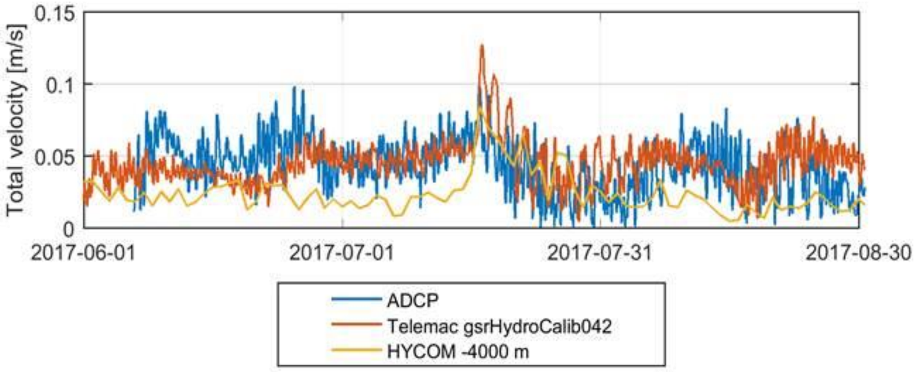

Supplementary Figure 8. *Comparison between the TELEMAC model current velocity magnitude, real ADCP data from the CCFZ, and the HYCOM model results at 4,000 m of depth. The ADCP data was measured in the CCFZ Belgian exploration area (14º 9.7'N 125º 53.55'W) at 4,000 m of depth with a 300 kHz Teledyne RDI workhorse ADCP. Note that the HYCOM fields do not include the tidal component.*

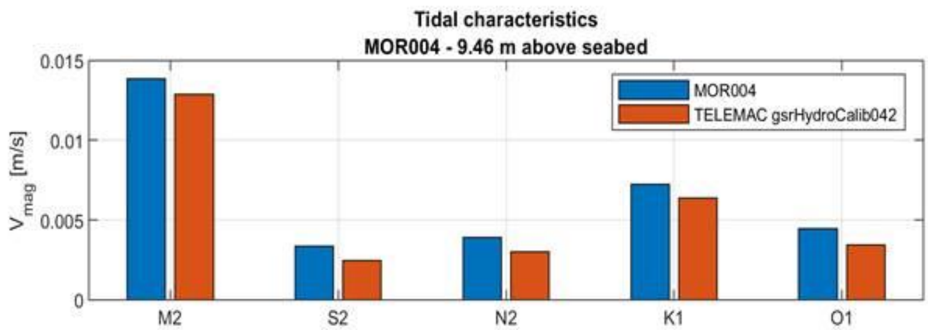

Supplementary Figure 9. *Comparison of the tidal characteristics above the seabed obtained by the TELEMAC model, with those obtained from the ADCP data in the Belgian exploration area (14º 9.7'N 125º 53.55'W) presented in Supplementary Figure 7.*

Supplementary Notes 2

Analytical validation of advection-diffusion in the TELEMAC model

When exposed to a relatively constant and uniform background current, the sediment concentration of a plume released from a localized source is mainly controlled by advection away from the source, as well as turbulent diffusion in the plane normal to the direction of advection. The advection velocity controls the initial dilution of the plume discharge by stretching or contracting the volume of carrying fluid going through the source per unit time. For a source of sediment with a mass discharge rate $\dot{m} = c_p Q$, where c_p (kg m^{-3}) is the concentration in the pipe and Q (m^3 s^{-1}) is the flow rate, subjected to a uniform flow U (m s^{-1}), the resulting plume has a mass per unit length $M = \dot{m}/U$. This mass is spread over the initial area of the plume of height H and width W such that the plume as an initial concentration $c_0 = \frac{M}{HW}$.

Once the initial dilution caused by advection is set, the plume evolves primarily under the influence of horizontal diffusion, and to a lesser extent from vertical diffusion. For the initial conditions of a rectangular plume of height H, width W and concentration c_0 centered on $y = z = 0$, the analytical solution to the two-dimensional diffusion problem is equation (S1).

$$c(t,y,z) = \frac{c_0}{4}\left(\operatorname{erf}\left(\frac{y+\frac{W}{2}}{\sqrt{4\kappa_y t}}\right) - \operatorname{erf}\left(\frac{y-\frac{W}{2}}{\sqrt{4\kappa_y t}}\right)\right) \times \left(\operatorname{erf}\left(\frac{z+\frac{H}{2}}{\sqrt{4\kappa_z t}}\right) - \operatorname{erf}\left(\frac{z-\frac{H}{2}}{\sqrt{4\kappa_z t}}\right)\right), \quad \text{(S1)}$$

where y is the coordinate in the direction normal to the direction of advection in the horizontal plane and z is the vertical coordinate. The extent x_t of contours of dilution $\frac{c_p}{c_t} = 10^4$, 4×10^4, 10^5 and 4×10^5 are computed from supplementary equation (S1) and compared to the results from the TELEMAC model for the parameters $Q = 0.56\, m^3\ s^{-1}$, $c_p = 8.3 kg\, m^{-3}$, $\kappa_y = 0.3 m^2\ s^{-1}$, $\kappa_z = 0.033\, m^2\ s^{-1}$, $W = 200m$, $H = 100m$, and using the current velocity and heading from the TELEMAC model shown in Supplementary Figure 7 to advect the plume (Supplementary Figure 10).

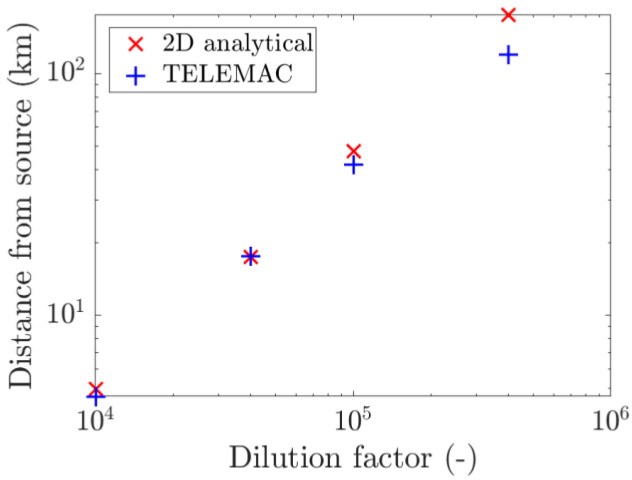

Supplementary Figure 10. *Comparison between the 2D diffusion analytical solution and the TELEMAC model results for the 10,000, 40,000, 100,000 and 400,000 dilution factors on day 36 of the simulation. Excellent agreement is found between the TELEMAC simulations and the two-dimensional analytical diffusion model for dilution contours of 10^4, 4 x 10^4, 10^5, and 4 x 10^5. The distance from the source is measured as the length of the plume centerline from the source to the end of the dilution contour.*

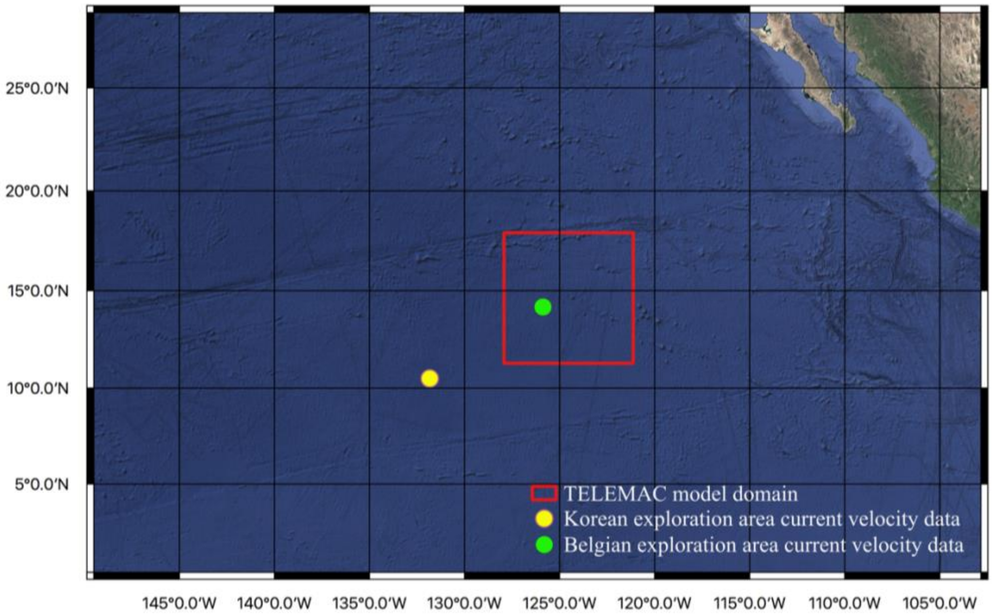

Supplementary Figure 11. *Map including the CCFZ, the TELEMAC model domain (red box), the location of the current velocity from the Belgian area (green dot) used for the model validation (Supplementary Figures 8 and 9), and location of the current velocity time series from the Korean exploration area (yellow dot) (Supplementary Figure 1). Map background source: Google (2020).*

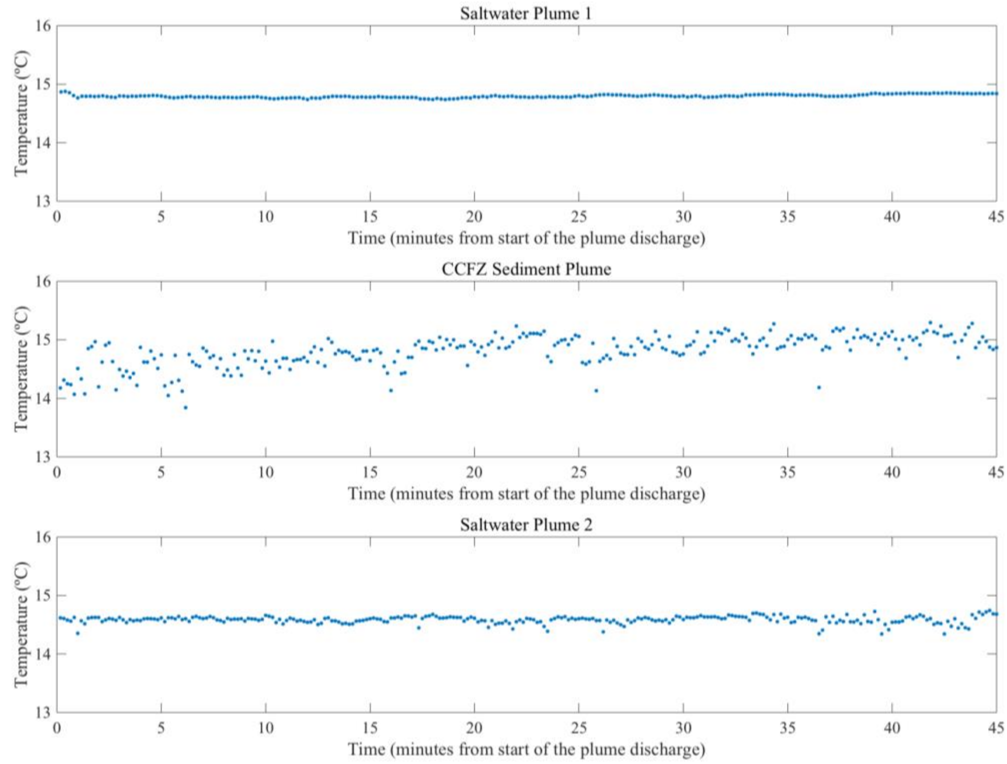

Supplementary Figure 12*. Time series of plume temperature at the nozzle during the discharge of the three experimental plumes, as measured by the SBE56 thermistor.*

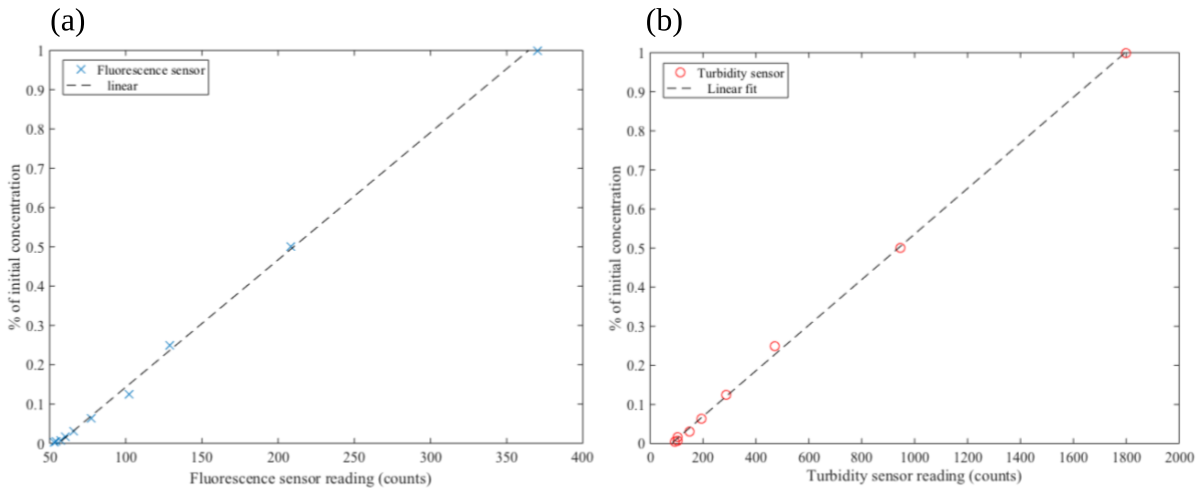

Supplementary Figure 13. *Calibration curves of the ECO Triplet scattering fluorescence (rhodamine) (a) and turbidity (b) sensor signals. During the calibration procedure, each calibration sample was measured three times during a period of one minute. The average of the three one-minute measurements is the value used to build the calibration curve. As expected, the calibration curve presents a clear linear trend.*

Supplementary Notes 3

MIT-MSEAS modeling system results description

The MIT-MSEAS modeling system demonstrated real-time forecasting skill starting from February 23 until March 5, 2018, issuing forecasts daily and for a 2.5-day duration. Forecasts were validated against several independent data sets in real-time, as soon as synoptic data became available. The comparison to ship CTD profiles from R/V Sally Ride showed that the forecast temperature and salinity aligned well with these data, with the mean and maximum error at 60 m being approximately 0.2 and 0.4°C for temperature and 0.025 and 0.06PSU for salinity. The validation against glider profiles from Scripps showed that mean and maximum errors at 60 m were approximately 0.3 and 1.1°C for temperature and 0.03 and 0.085PSU for salinity. Comparison of forecasts with satellite data were also very good. In summary, the MSEAS forecasts had skill at all depths for the whole PLUMEX and forecast errors were much smaller than the variability in the region.

As presented in Figure 4, the multi-resolution MIT-MSEAS modeling system was run in real-time, predicting that the plume traveled ~0.44 km to the south-southwest in the first 80 minutes, followed by a southeastward motion of ~0.34 km in the following 40 minutes. The plume then again traveled south-southwest for ~0.49 km in the next 130 minutes. The final plume location was predicted to be ~1.39 km to the south of the initial release point 370 minutes after the plume release. The forecasted plume locations matched well with the actual measurements. The distances between the centroids of the forecasted plumes and the corresponding plume detections during the tow-yo (which are located on top of the ship track) 78, 120, 250 and 371 minutes after the start of the plume release were 0.16 km, 0.13 km, 0.25 km, and 0.17 km, respectively. Note that these deviations are of the order of the size of a single grid cell. The multi-resolution MSEAS forecasting system was thus able to predict the general trend of the plume transport, even though the oceanographic data were limited (only a few CTD profiles were employed and the ADCP data were not available nor assimilated in real-time). Considering that the MIT-MSEAS modeling system did not use the ADCP data, the obtained results are promising for future modeling integrated with plume monitoring.

Supplementary Notes 4

Simplified model of sedimentation from a midwater discharge

An operation with an annual production of 3 million tonnes of dry nodules operating 260 days per year has been estimated to discharge about 5.4 kg s^{-1} of sediment and 2.7 kg s^{-1} of nodules fines in the form of a midwater plume[18] from the mining vessel. Based on the estimated loads of sediments and fines, one mining operation would discharge a total of ~1.2x10^8 kg of sediment (M_s) and ~6.1x10^7 kg of fines (M_f) into the ocean per year.

A 10µm particle with a 0.1 mm s^{-1} settling velocity takes about 405 days to settle 3500 m from the initial ambient plume depth to the seabed. Over that period of time and with an average current velocity of 4 cm s^{-1}, a particle may travel up to 1400 km before reaching the seabed. One can assume that over the 20 years of operation of a nodule mining exploitation, the ocean current variability results in a somewhat even distribution of particles and fines over a circle with a radius (R) on the order of 1000 km.

Based on these assumptions, it is possible to estimate the average yearly sedimentation rate (S) for a nodule mining operation as $S = (M_s/\rho_s + M_f/\rho_f)/A$, where ρ_s is the density of the sediment particles (2600 kg m^{-3}), ρ_f is the density of the nodule fines (3400kg m^{-3}), and A is the area where the particles uniformly settle (for a circle of radius R: $A = \pi R^2$). Supplementary Table 1 presents results for the discharge from 1, 5, 10 and 20 nodule mining operations settling in a 1000 km radius circular area. The average yearly sedimentation rate ranges from 2.3x10^{-3} µm per year to 4.1x10^{-1} µm per year compared to background sedimentation rates of 1 µm per year[17].

Furthermore, it is possible to estimate the volume of water affected by a sediment concentration above a certain threshold at any given point in time and over one year using the simple analytical model introduced in Supplementary Material 8 (equation (S1)). The results included in Supplementary Table 1 assume a uniform settling velocity, $\kappa_y = 0.3\, m^2\ s^{-1}$, $\kappa_z = 0.033\, m^2\ s^{-1}$, $W = 200\, m$ and $H = 100\, m$.

Supplementary Table 1. *Estimation of average yearly sedimentation rate and volume of ocean water with sediment concentration above 200 and 20 μg L^{-1} at any given time, and over a period of one year for discharges from 1, 5, 10 and 20 simultaneous nodule mining operations, assuming an annual production of 3 million tons of dry nodules operating 260 days per year. For the sedimentation rate calculation, particles are assumed to spread somewhat uniformly on a circular area of radius 1000 km over the course of 20 years. The sedimentation rate calculation assumed sediment and fines densities of 2600 kg m^{-3} and 3400 kg m^{-3}, respectively, and a 100% sediment and fines content in the deposited layer. For comparison, the background sedimentation rate in the CCFZ is 1 μm per year[17] and the total volume of water in the CCFZ at any given time is around 18 million km^3.*

Number of simultaneous nodule mining operations in the CCFZ	1	5	10	20
Sediment mass flux per operation (kg s^{-1}) [18]	5.4	5.4	5.4	5.4
Fines mass flux per operation (kg s^{-1}) [18]	2.7	2.7	2.7	2.7
Annual sediment mass flux (kg per year)	1.2×10^8	6.1×10^8	1.2×10^9	2.4×10^9
Annual fines mass flux (kg per year)	6.1×10^7	3.0×10^8	6.1×10^8	1.2×10^9
Sedimentation rate assuming uniform spread over a disk of 1000 km radius (μm per year)	2.1×10^{-2}	1.0×10^{-1}	2.1×10^{-1}	4.1×10^{-1}
Volume of ocean water with sediment concentration above 200 μg L^{-1} (km^3)	6.8	34	68	136
Volume of ocean water with sediment concentration above 20 μg L^{-1} (km^3)	680	3400	6800	13600
Annual volume of ocean water with sediment concentration above 200 μg L^{-1} (km^3 per year)	335	1675	3350	6700
Annual volume of ocean water with sediment concentration above 20 μg L^{-1} (km^3 per year)	3350	16750	33500	67000